Original Article

Mol Imaging Radionucl Ther **DOI:***10.4274/mirt.galenos.2026.80037*

[Epub Ahead of Print]

Comparative Performance of ^{18}F-FDG PET/CT and ^{68}Ga-FAPI PET/CT in TENIS Syndrome in Treated Differentiated Thyroid Carcinoma

Tedavi Edilmiş Diferansiye Tiroid Karsinomunda TENIS Sendromunda ^{18}F-FDG PET/CT ve ^{68}Ga-FAPI PET/CT'nin Karşılaştırmalı Performansı

Jayantilal Bhagirath Bhad[1], Manjit Sarma[1], Usha Menon[2], Ramkesh R.[1], Parvathy Pavithran[1], Awiral Saxena[1], Sanjana Sajeev[1], B. Venkata Sai Ram Reddy[1], Padma Subramanyam[1], Shanmuga Sundaram P[1]

[1]*Amrita Institute of Medical Sciences and Research (Amrita Vishwavidyapeetham), Department of Nuclear Medicine and Molecular Imaging, Kochi, India*

[2]*Amrita Institute of Medical Sciences and Research (Amrita Vishwavidyapeetham), Department of Endocrinology, Kochi, India*

Abstract

Objectives: Thyroglobulin-elevated negative iodine scintigraphy (TENIS) syndrome presents a significant diagnostic challenge in the management of differentiated thyroid carcinoma (DTC). Although ^{18}F-fluorodeoxyglucose positron emission tomography/computed tomography (^{18}F-FDG PET/CT) is the established imaging modality for detecting presence of structural disease, Gallium-68 (^{68}Ga)-fibroblast activation protein inhibitor (FAPI) PET/CT, which targets the tumor stroma, represents a promising new alternative. This study directly compared the lesion detection capabilities of both tracers in patients with TENIS.

Methods: In this prospective single-center study (2021-2024), 22 patients with TENIS syndrome underwent both ^{18}F-FDG and ^{68}Ga-FAPI PET/CT scans within a 7-day interval of each other. Lesion detectability and maximum standardized uptake values (SUV_{max}) were compared between the two modalities. Lesions were validated using histopathology or cytopathology, biochemical response to empirical ^{131}I therapy, imaging correlation or progression, and clinical progression methods.

Results: Among 22 patients (median age 43.5 years, 90% with papillary carcinoma), ^{18}F-FDG was positive in 23/33 cervical lymph nodes, whereas ^{68}Ga-FAPI was positive in 14/33 lymph nodes. Fourteen lymphnodes were positive on both modalities with comparable SUV_{max} (median ^{18}F-FDG 3.3 vs. ^{68}Ga-FAPI 3.6, p=0.689). All local recurrences in thyroid bed (n=4) were ^{18}F-FDG-positive, whereas only 3 of the local recurrences were ^{68}Ga-FAPI-positive. Distant metastases (lung and bone) showed similar detection rates.

Conclusion: ^{18}F-FDG PET/CT demonstrates superior lesion detectability, particularly for cervical lymph nodes, in TENIS syndrome. ^{68}Ga-FAPI PET/CT provides complementary information with comparable semiquantitative uptake in detected lesions but with lower overall detection. ^{18}F-FDG PET/CT remains the preferred imaging modality for comprehensive disease evaluation in patients with radioactive iodine-refractory DTC.

Keywords: TENIS syndrome, well differentiated thyroid carcinoma, ^{18}F-FDG PET, ^{68}Ga-FAPI PET, positron emission tomography computed tomography

Address for Correspondence: Manjit Sarma, Amrita Institute of Medical Sciences and Research (Amrita Vishwavidyapeetham), Department of Nuclear Medicine and Molecular Imaging, Kochi, India

E-mail: drmanjitsarma@gmail.com **ORCID ID:** orcid.org/0000-0002-4086-4423

Received: 30.01.2026 **Accepted:** 21.06.2026 **Epub:** 18.08.2026

Cite this article as: Bhagirath Bhad J, Sarma M, Menon U, R. R, Pavithran P, Saxena A, Sajeev S, Reddy B.VSR, Subramanyam P, Sundaram P S. Comparative performance of ^{18}F-FDG PET/CT and ^{68}Ga-FAPi PET/CT in TENIS syndrome in treated differentiated thyroid carcinoma. Mol Imaging Radionucl Ther. .

Öz

Amaç: Tiroglobulin yüksekliği olan negatif iyot sintigrafisi (TENIS) sendromu, diferansiye tiroid karsinomu (DTC) yönetiminde önemli bir tanısal zorluk oluşturmaktadır. Yapısal hastalığın varlığını saptamada ^{18}F-florodeoksiglukoz pozitron emisyon tomografisi/bilgisayarlı tomografi (^{18}F-FDG PET/CT) yerleşik görüntüleme yöntemi olmakla birlikte, tümör stromasını hedefleyen Galyum-68 (^{68}Ga)-fibroblast aktivasyon proteini inhibitörü (FAPI) PET/CT umut vadeden yeni bir alternatif olarak öne çıkmaktadır. Bu çalışmada, TENIS hastalarında her iki izleyicinin lezyon saptama kapasiteleri doğrudan karşılaştırılmıştır.

Yöntemler: Bu prospektif tek merkezli çalışmada (2021-2024), TENIS sendromu olan 22 hastaya, birbirinden 7 gün arayla ^{18}F-FDG ve ^{68}Ga-FAPI PET/CT görüntülemeleri uygulanmıştır. İki yöntem arasında lezyon saptanabilirliği ve maksimum standartlaştırılmış tutulum değerleri (SUV_{max}) karşılaştırılmıştır. Lezyonlar; histopatoloji veya sitopatoloji, ampirik ^{131}I tedavisine biyokimyasal yanıt, görüntüleme korelasyonu veya progresyonu ve klinik progresyon yöntemleri kullanılarak doğrulanmıştır.

Bulgular: Yirmi iki hasta arasında (ortanca yaş 43,5 yıl; %90'ı papiller karsinom), ^{18}F-FDG 33 servikal lenf nodunun 23'ünde pozitif saptanırken, ^{68}Ga-FAPI 33 lenf nodunun 14'ünde pozitif saptanmıştır. On dört lenf nodu her iki yöntemde de pozitif bulunmuş ve SUV_{maks} değerleri benzerlik göstermiştir (ortanca ^{18}F-FDG: 3,3; ^{68}Ga-FAPI: 3,6; p=0,689). Tiroid yatağındaki tüm lokal nüksler (n=4) ^{18}F-FDG pozitif iken, lokal nükslerin yalnızca 3'ü ^{68}Ga-FAPI pozitif bulunmuştur. Uzak metastazlarda (akciğer ve kemik) benzer saptama oranları gözlenmiştir.

Sonuç: ^{18}F-FDG PET/CT, TENIS sendromunda özellikle servikal lenf nodları açısından daha üstün lezyon saptanabilirliği göstermektedir. ^{68}Ga-FAPI PET/CT, saptanan lezyonlarda karşılaştırılabilir yarı kantitatif tutulum değerleriyle tamamlayıcı bilgi sağlamakla birlikte, genel saptama oranı daha düşüktür. Radyoaktif iyoda refrakter diferansiye tiroid karsinomu olan hastalarda kapsamlı hastalık değerlendirmesi için ^{18}F-FDG PET/CT tercih edilen görüntüleme yöntemi olmaya devam etmektedir.

Anahtar Kelimeler: TENIS sendromu, iyi diferansiye tiroid karsinomu, ^{18}F-FDG PET, ^{68}Ga-FAPI PET, pozitron emisyon tomografisi/bilgisayarlı tomografi

Introduction

Thyroid cancer (TC) is the most prevalent endocrine malignancy, accounting for nearly 95% of endocrine neoplasms worldwide (1). Most cases are classified as differentiated thyroid carcinoma (DTC), including papillary and follicular subtypes (2). The standard management of DTC consists of total or near-total thyroidectomy, often followed by radioactive iodine (RAI) ablation and thyroid-stimulating hormone (TSH) suppression in intermediate- or high-risk patients, as recommended by the American Thyroid Association (ATA) guidelines (3,4). With appropriate management, patients with DTC frequently achieve a favorable prognosis, with reported 10-year disease-specific survival rates approaching 98% (5,6).

Nevertheless, a subset of patients encounters persistent or recurrent disease, manifested biochemically by elevated serum thyroglobulin (Tg ≥1 ng/mL while suppressed or ≥ 10 ng/mL after stimulation), with or without positive anti- Tg antibodies, even in the absence of structural evidence of disease (6,7). Approximately 20% of these patients eventually develop structural recurrence, which is associated with a worse prognosis (6). Moreover, between 5% and 15% of DTC and up to 50% of metastatic lesions evolve into radioiodine-refractory (RAIR) disease, characterized by loss of radioiodine avidity and more aggressive clinical behavior (8,9).

A clinically significant manifestation of RAIR-DTC is thyroglobulin-elevated, negative iodine scintigraphy (TENIS) syndrome, which is encountered in up to 27% of post-treatment DTC cases (10). Patients with TENIS have elevated Tg levels despite negative radioiodine whole-body scans, implying iodine-non-avid, active disease (11). This scenario presents a diagnostic and management challenge because conventional radioiodine imaging fails to localize the disease (10,11).

The ATA guidelines recommend 2-^{18}F-Fluorodeoxyglucose positron emission tomography/computed tomography (^{18}F-FDG PET/CT) for patients with TENIS to localize metabolically active sites of recurrence/metastasis (3,4). The underlying rationale is the "flip-flop phenomenon," i.e., the inverse relationship between iodine and glucose avidity in TC, in which dedifferentiated tumour cells lose iodine transport capacity but acquire increased glucose metabolism, rendering them detectable by ^{18}F-FDG PET/CT (12,13). In well-differentiated, iodine-avid tumors, ^{18}F-FDG uptake is low, but it increases in dedifferentiated and aggressive lesions (12,14). The sensitivity of ^{18}F-FDG PET/CT in TENIS has been reported to be 68.8-87%, with false-negative rates of 8-21% depending on the disease burden and metabolic characteristics (12,15).

Recent advances have introduced fibroblast activation protein inhibitor (FAPI) labelled radiotracers that target cancer-associated fibroblasts abundant in the tumor stroma. Multiple FAPI compounds, such as FAPI-02, FAPI-04, and FAPI-46, are available, with Gallium-68 (^{68}Ga) labelling providing compatibility with clinical PET imaging (16). ^{68}Ga-FAPI PET/CT can detect lesions, irrespective of cellular differentiation or iodine avidity (16,17). Importantly, stroma and FAP expression are major features

of papillary and follicular thyroid carcinomas, particularly in dedifferentiated or aggressive disease, providing a rationale for ^{68}Ga-FAPI PET application in this setting (18,19).

While several studies have demonstrated strong ^{68}Ga-FAPI uptake in metastatic or thyroid bed recurrent RAIR-DTC lesions, others have suggested variable results, especially in well-differentiated or low-stroma tumors (20). A recent head-to-head comparison in RAIR-DTC showed that ^{68}Ga-FAPI detected additional lesions in approximately 20% of cases missed by ^{18}F-FDG, with higher target-to-background ratios (21). However, comprehensive comparative data on TENIS syndrome remain limited. Therefore, the comparison of ^{68}Ga-FAPI and ^{18}F-FDG PET/CT in TENIS remains an active area of clinical investigation.

Materials and Methods

Study Design and Patient Selection

This prospective, single-center study was conducted at a tertiary referral university-affiliated teaching hospital between 2021 and 2024. The study protocol was approved by the Amrita Institute of Medical Sciences and Research Institutional Clinical Research Ethics Committee, and written informed consent was obtained from all participating patients. This study conformed to the ethical guidelines of the 2013 revision of the Declaration of Helsinki.

Eligible patients were adults aged ≥18 years with histopathologically confirmed DTC who had previously undergone total or near-total thyroidectomy, received adjuvant ^{131}I ablation, and subsequently developed TENIS syndrome. The inclusion criteria required documented elevated serum Tg levels (stimulated Tg ≥10 ng/ml or further rising trend of stimulated Tg level in patients with previously documented stimulated Tg ≥2 ng/ml), and a negative diagnostic ^{131}I scan. The exclusion criteria were the presence of a second primary malignancy or refusal to provide informed consent.

PET/CT Acquisition Protocol

All PET/CT examinations were performed using a Siemens Biograph Horizon PET/CT system (Siemens Healthineers, Germany) equipped with lutetium oxyorthosilicate detectors and time-of-flight (TOF) reconstruction. Each patient underwent both ^{18}F-FDG and ^{68}Ga-FAPI PET/CT within seven days (median interval: 2 days). Patients fasted for at least six hours before ^{18}F-FDG PET/CT. Blood glucose was measured prior to radiotracer injection and was required to be <150 mg/dl. Intravenous ^{18}F-FDG was administered at a dose of 3.7 MBq/kg , followed by whole-body images (skull base to mid-thigh) acquired 45-60 min post-injection, with one minute per bed position. For FAPI PET/CT, the patients received an intravenous injection of 1.8-2.2 MBq/kg ^{68}Ga-FAPI-04. Imaging was initiated 30-45 min post-injection, using the same anatomical range but with a two-minute acquisition per bed position. A low-dose, non-contrast CT scan (130 kV, 110-130 mAs, 3 mm slice thickness) was acquired for attenuation correction and anatomical localization, followed by a three-dimensional PET acquisition. Images were reconstructed using the ordered-subsets expectation-maximization + TOF algorithm (3 iterations × 10 subsets) with CT-based attenuation and scatter correction. The data were reviewed using the syngo MI Workplace software suite (Siemens Healthineers).

Image Analysis

The images were independently reviewed by two board-certified, experienced nuclear medicine physicians blinded to the clinical and laboratory information and each other's interpretations. Discrepancies were resolved through consensus. Lesions were considered positive on PET if they showed focal ^{18}F-FDG or ^{68}Ga-FAPI uptake exceeding the background without a physiological explanation. Semi-quantitative analysis involved manual delineation of regions of interest around each lesion to obtain the maximum standardized uptake value (SUV_{max}). Lesions on CT without PET positivity were considered pathological if they fulfilled CT criteria for disease involvement.

Lesion Confirmation and Validation

We employed a hierarchical multimodal approach for lesion validation. Whenever feasible, lesions were confirmed by surgical excision with histopathological examination, or by fine-needle aspiration cytology. This represents the gold standard for confirmation. For lesions that could not be biopsied, the biochemical response to empirical ^{131}I therapy was used as a surrogate marker. Decreases in stimulated Tg levels following therapy are considered supportive evidence of both disease presence and treatment response. Recurrent lesions in the thyroid bed were corroborated by correlative ultrasound imaging, which demonstrated the characteristic features of recurrent TC. Imaging features suggestive of metastatic disease were used to identify distant lesions. Serial follow-up imaging (PET/CT, CT, or magnetic resonance imaging) demonstrating interval growth or increased metabolic activity of the lesions was also considered confirmatory evidence. Clinical deterioration with new or worsening symptoms (e.g., bone pain and respiratory symptoms), corroborated by imaging findings, was used to validate lesion significance. This multimodal confirmation strategy provided validation despite the practical limitations of performing histopathological sampling in all patients with advanced diseases.

Data Collection

Clinical and laboratory data were systematically collected from electronic hospital medical records and included: patient demographics (age and sex), histopathological subtype and grade, initial surgical treatment, number of ^{131}I therapy cycles, cumulative radioiodine dose, and serial stimulated serum Tg and anti-Tg antibody (TgAb) measurements (measured at initial diagnosis, at TENIS detection, and post-therapy). The imaging data included lesion location, lesion size on anatomical CT, and SUV_{max} on both ^{18}F-FDG and ^{68}Ga-FAPI PET/CT. Follow-up data included subsequent management (surgery, empirical radioiodine therapy), histopathological confirmation results, serial imaging findings, biochemical response assessments, and clinical outcomes.

Statistical Analysis

Continuous variables are presented as medians (ranges), and categorical variables are presented as counts (percentages). Paired comparisons of SUV_{max} in lesions positive on both modalities were performed using the Wilcoxon signed-rank test. Statistical significance was set at $p<0.05$.

Results

Patient Characteristics

This study included 22 TENIS patients. The median age was 43.5 years (range, 21-79 years), and 63% were female. Most cases (90%) were identified as papillary thyroid carcinoma, while follicular and poorly differentiated/microcarcinoma accounted for the remaining 10%. Most patients (59%) underwent total thyroidectomy, while 37% also underwent lymph node dissection. Eleven patients (50%) received one cycle of ^{131}I therapy, and the remaining 11 patients (50%) received two cycles; the median cumulative radioiodine dose was 118.5 mCi (range, 60-215 mCi). The initial median Tg and anti-TgAb levels were 50.48 ng/ml and 28.07 IU/ml, respectively. Most patients (86%) had Tg levels above 10 ng/mL, and most were at intermediate risk on initial assessment. Patient characteristics are shown in Table 1.

Lesion Confirmation

Lesion validation followed a hierarchical multimodal approach. The validation methods by lesion type are summarized in Table 2. Cervical lymph node involvement was confirmed by histopathology or cytopathology in 75% (9 of 12 patients), providing high confidence in nodal disease findings. Local recurrences and distant metastatic lesions were confirmed primarily by biochemical response, imaging findings, and clinical progression, reflecting the practical challenges of invasive sampling at these anatomical sites.

Local thyroid bed recurrent lesions

CT imaging identified local recurrence in 4 of 22 patients. In all four patients, the lesions were ^{18}F-FDG-avid, whereas in three patients the lesions were ^{68}Ga-FAPI-positive (Figure 1).

Table 1. Patient characteristics (n=22)

Characteristic	Value
Median age, years (range)	43.5 (21-79)
Sex, n (%)	
Female	14 (63%)
Male	8 (37%)
Histopathologic features	
Pathologic subtype, n (%)	
Papillary	20 (90%)
Follicula	1 (5%)
Poorly differentiated + microcarcinoma	1 (5%)
Initial treatment	
Initial surgery, n (%	
Total thyroidectomy + LN dissection	8 (37%)
Total thyroidectomy only	13 (59%)
Subtotal thyroidectomy	1 (4%)
^{131}I therapy cycles, n (%)	
1 cycle	11 (50%)
2 cycles	11 (50%)
Cumulative ^{131}I dose, mCi (range)	118.5 (60-215)
Biochemical parameters	
Tg at initial diagnosis, ng/ml (range)	50.48 (0.8-925.9)
Tg-Ab at initial diagnosis, IU/ml (range)	28.07 (1.25-4000)
Tg at TENIS detection, ng/ml (range)	42.22 (0.04-274)
Tg-Ab at TENIS detection, IU/ml (range)	28.07 (1.25-4000)
Tg post-therapy (n=21), n (%)	
0-10 ng/ml	3 (14%)
>10 ng/ml	18 (86%)
Tg-Ab post-therapy (n=21), n (%)	
Positive	5 (24%)
Negative	16 (76%)
Risk stratification	
Initial risk stratification (n=21), n (%)	
Low	3 (14%)
Intermediate	16 (76%)
High	2 (10%)

LN: Lymph node, Tg: Thyroglobulin, Tg-Ab, anti-thyroglobulin antibody, TENIS: Thyroglobulin-elevated negative iodine scintigraphy

One ^{18}F-FDG-avid lesion (SUV_{max} 3.2) was negative on ^{68}Ga-FAPI PET/CT imaging. The median ^{18}F-FDG SUV_{max} for local recurrence was 4.45 (range, 3.2-6.8), and the median ^{68}Ga-FAPI SUV_{max} was 2.9 (range, 2.4-10.5). The SUV metrics are presented in Table 3.

Lymph Node Metastases

Among the 33 lymph nodes identified on CT imaging, ^{18}F-FDG was positive in 23 nodes (69.7%), whereas ^{68}Ga-FAPI was positive in 14 nodes (42.4%) (Figure 2). Fourteen nodes were positive on both modalities and analyzed in

Table 2. Lesion validation methods by lesion type

Lesion type	Number of patients (n=)	Confirmation method
Cervical lymph nodes	n=12	Histopathology/FNAC (n = 9), Tg changes post empirical ^{131}I (n=2), clinical progression (n=1)
Local recurrence	n=2	Tg changes post empirical ^{131}I (n=1), correlative ultrasound imaging (n=1)
Pulmonary nodules	n=4	Imaging progression on follow-up (n=2), imaging correlation (n=1), clinical progression (n=1)
Skeletal lesions	n=1	Clinical progression (n=1)

FNAC: Fine-needle aspiration cytology, Tg: Thyroglobulin

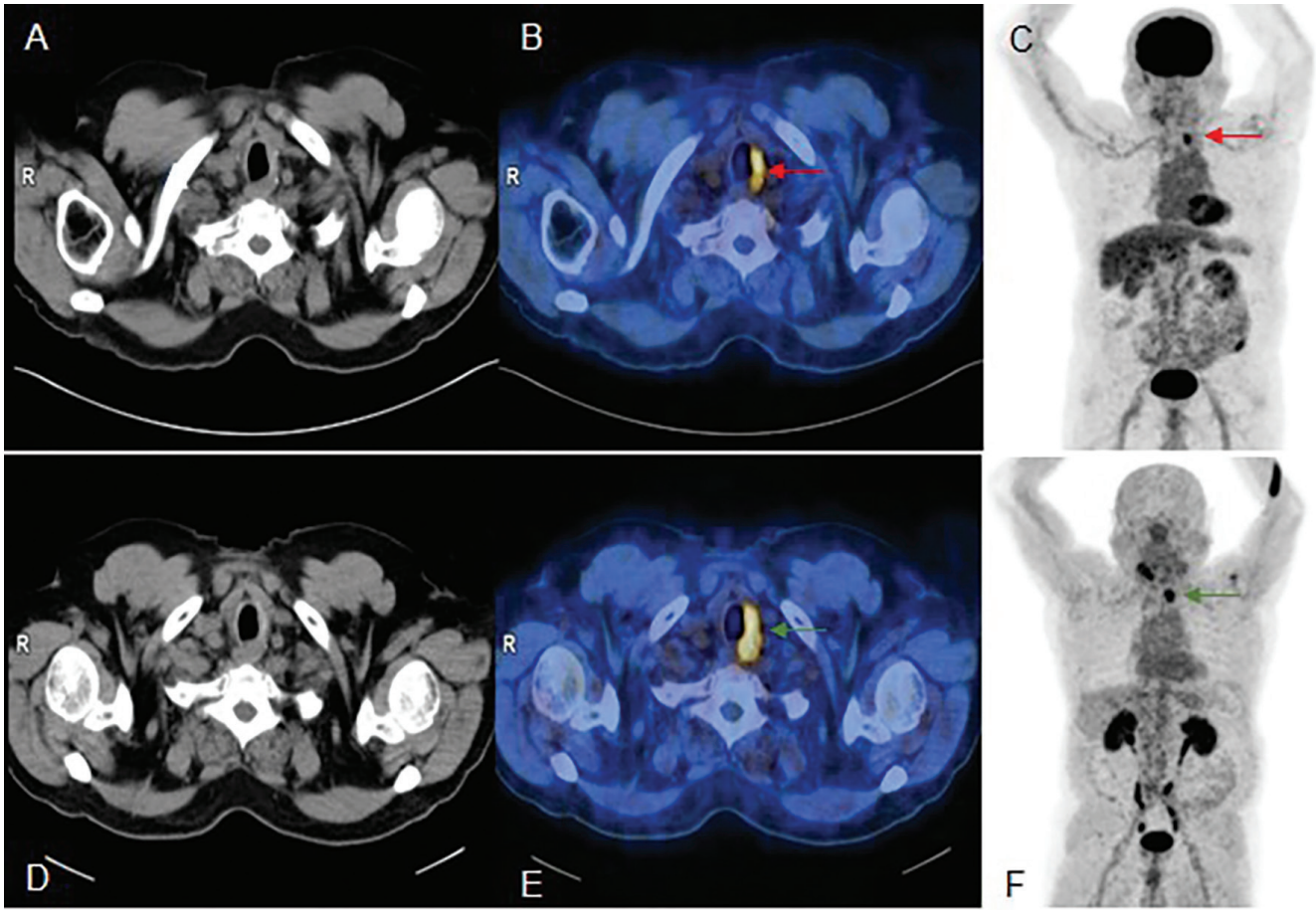

Figure 1. Detection of local recurrence in the thyroid bed. (A, D) axial non contrast CT shows an ill-defined soft-tissue lesion in thyroid bed on left side. (B) Selected axial fused images demonstrating moderate ^{18}F-FDG uptake (SUV_{max}, 6.8) (red arrow). (E) ^{68}Ga-FAPI PET shows intense uptake (SUV_{max} 10.5) in the soft tissue lesion suggesting a prominent stromal reaction (green arrow). (C, F) MIP images of ^{18}F-FDG PET and ^{68}Ga-FAPI PET Whole body PET showing focal increased ^{18}F-FDG and ^{68}Ga-FAPI in lower neck and physiological tracer distribution in rest of the whole body

^{18}F-FDG: ^{18}F-fluorodeoxyglucose, CT: Computed tomography, ^{68}Ga-FAPI PET: Gallium-68- fibroblast activation protein inhibitor positron emission tomography, SUV_{max}: Maximum standardized uptake value, MIP: Maximum intensity projection

paired comparisons of SUV_{max}. The median SUV_{max} was 3.3 (range 2.2-16.8) for ^{18}F-FDG and 3.6 (range 2.2-9.8) for ^{68}Ga-FAPI (Figure 3). The Wilcoxon signed-rank test showed no significant difference in SUV_{max} between ^{18}F-FDG and ^{68}Ga-FAPI in paired lymph-nodal lesions (p=0.689). ^{18}F-FDG PET/CT detected more lymph nodes overall than ^{68}Ga-FAPI PET/CT. The detailed metrics are presented in Table 4.

Distant Metastases

Five pulmonary lesions were identified on CT. ^{18}F-FDG was positive in all five lesions, whereas ^{68}Ga-FAPI was positive in four lesions (Figure 4). The median SUV_{max} was 3.3 for ^{18}F-FDG and 5.05 for ^{68}Ga-FAPI, respectively. Mean SUV_{max} was 5.72±5.75 for ^{18}F-FDG and 5.95±4.13 for ^{68}Ga-FAPI.

Table 3. SUV_{max} values for local recurrence lesions

Metric	^{18}F-FDG PET/CT	^{68}Ga-FAPI PET/CT
n (lesions)	4	3
Median SUV_{max} (range)	4.45 (3.2-6.8)	2.9 (2.4-10.5)
mean ± SD	4.73±1.69	5.27±4.54

FAPI: Fibroblast activation protein inhibitor, SUV_{max}: Maximum standardized uptake value, SD: Standard deviation, ^{18}F-FDG PET/CT: ^{18}F-fluorodeoxyglucose positron emission tomography/computed tomography

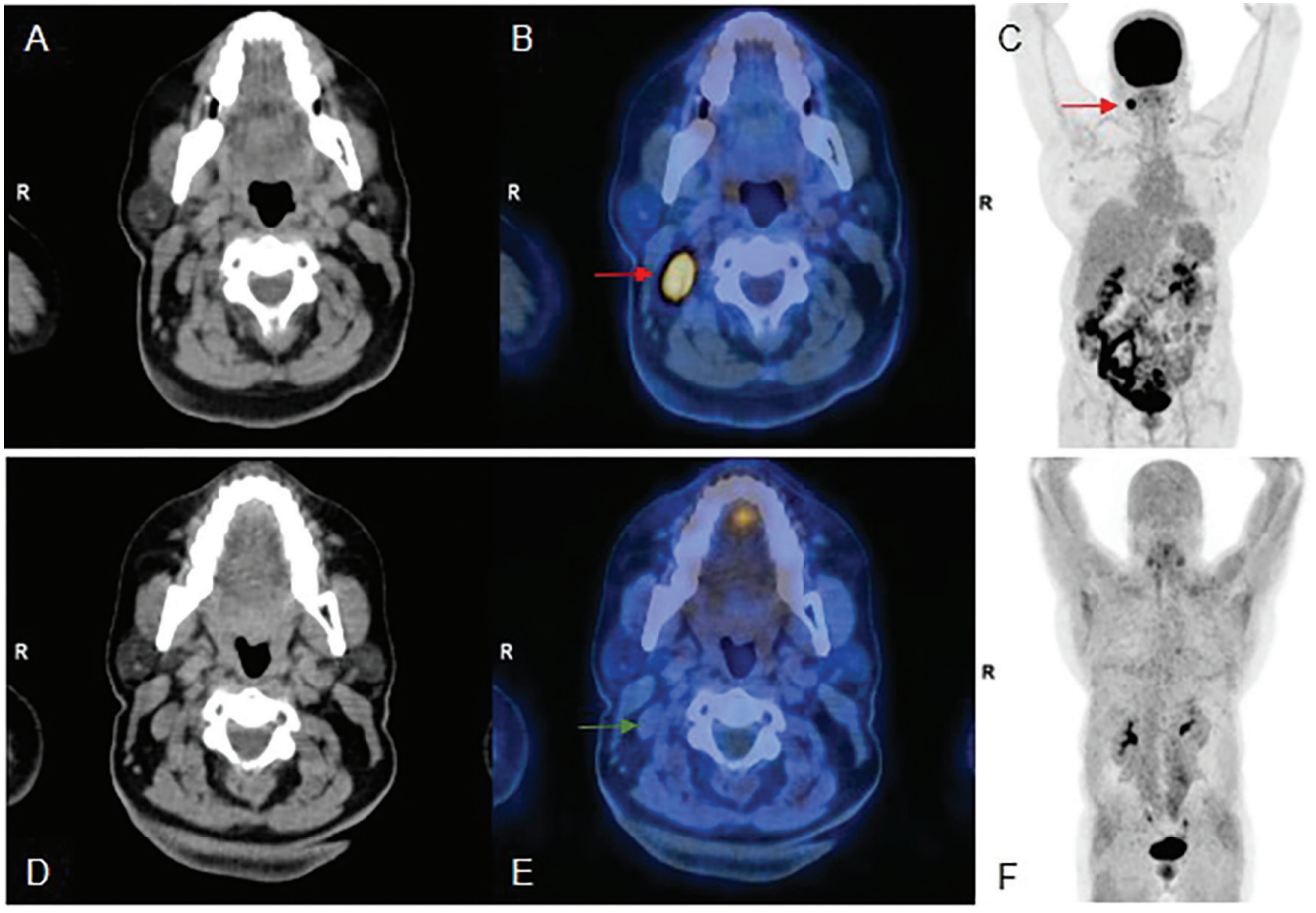

Figure 2. Superior lymphnodal detectability of ^{18}F-FDG PET. (A, D) axial non contrast CT showing an enlarged right level II cervical lymph node (B, E) selected axial fused images demonstrating ^{18}F-FDG positive node (red arrow) that was ^{68}Ga-FAPI negative (green arrow). (C, F) MIP images of ^{18}F-FDG PET and ^{68}Ga-FAPI PET Whole body PET showing focal increased ^{18}F-FDG in lower neck with no ^{68}Ga-FAPI positivity and physiological tracer distribution in rest of the whole body

^{18}F-FDG PET: ^{18}F-fluorodeoxyglucose positron emission tomography, CT: Computed tomography, ^{68}Ga-FAPI PET: Gallium-68- fibroblast activation protein inhibitor positron emission tomography, MIP: Maximum intensity projection

Two bone lesions were identified, both detected by ^{18}F-FDG and ^{68}Ga-FAPI PET/CT. The median SUV_{max} values were 4.75 for ^{18}F-FDG and 3.5 for ^{68}Ga-FAPI. The mean SUV_{max} was 4.75±0.64 for ^{18}F-FDG and 3.5±0.42 for ^{68}Ga-FAPI. The Wilcoxon signed-rank test comparing paired lung and bone lesions (n=6) showed no statistically significant difference in SUV_{max} (p=1.0). The detailed metrics are presented in Table 5.

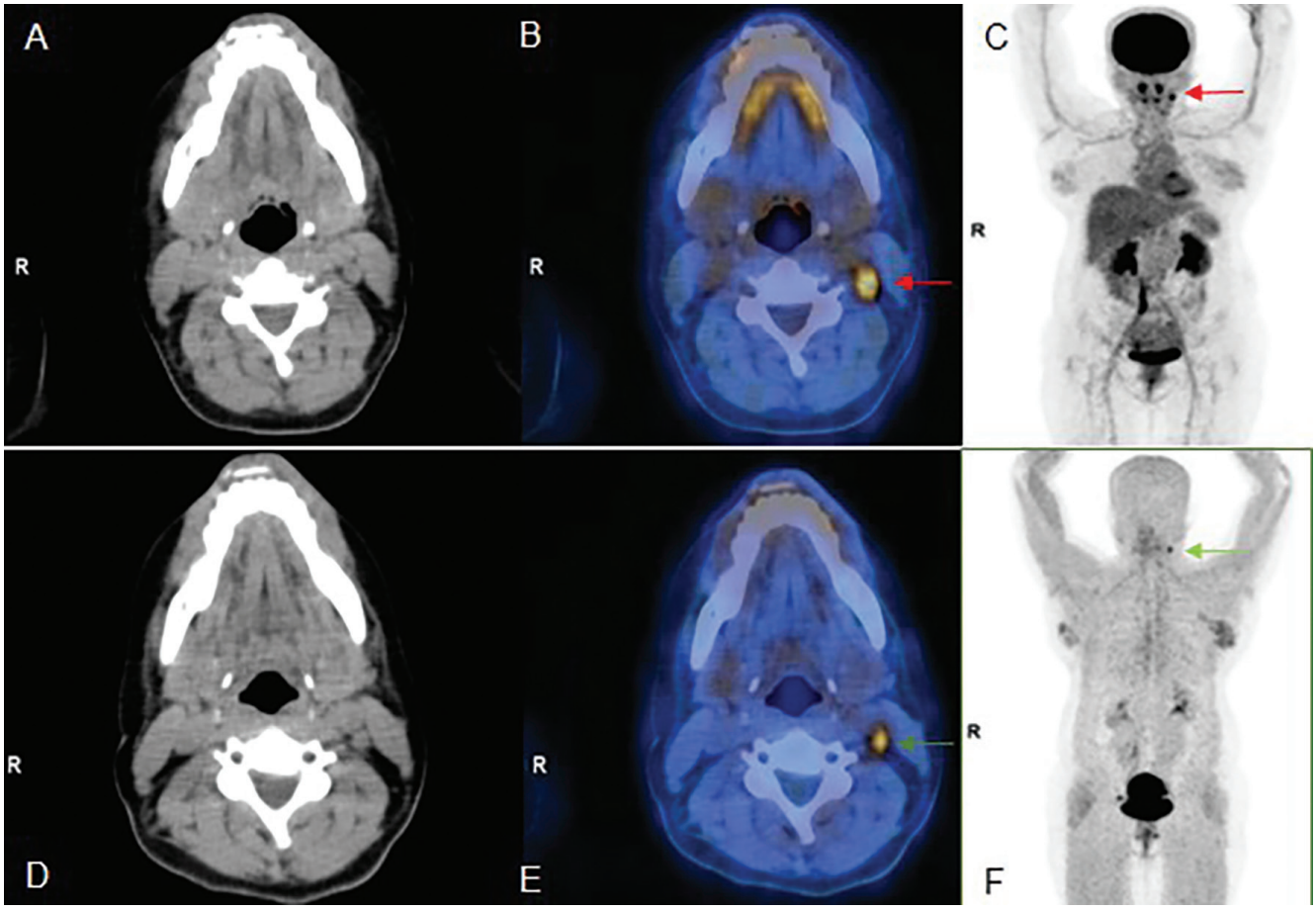

Figure 3. Lesser ^{68}Ga-FAPI avidity than ^{18}F-FDG avidity in a metastatic cervical lymphnode (A, D) axial CT image showing a metastatic left level II lymph node. (B) Corresponding fused ^{18}F-FDG PET image demonstrating intense metabolic activity in the lymphnode (SUV_{max} 9.8) (red arrow). (E) Fused ^{68}Ga-FAPI PET image showing moderate uptake (SUV_{max} 6.1) in the same node (green arrow). Histopathological examination of the surgical resection specimen confirmed metastatic papillary thyroid carcinoma. (C, F) MIP images of ^{18}F-FDG and ^{68}Ga-FAPI whole body PET showing focal increased ^{18}F-FDG and ^{68}Ga-FAPI uptake in upper cervical region on left side and physiological tracer distribution in rest of the whole body
^{18}F-FDG: ^{18}F-fluorodeoxyglucose, CT: Computed tomography, ^{68}Ga-FAPI PET: Gallium-68- fibroblast activation protein inhibitor positron emission tomography, SUV_{max}: Maximum standardized uptake value, MIP: Maximum intensity projection

Table 4. SUV_{max} values for lymph node metastases

Metric	^{18}F-FDG PET/CT	^{68}Ga-FAPI PET/CT	Paired lesions	Wilcoxon p-value
n (detected nodes)	23	14	14	—
Detection rate (%)	69.7%	42.4%	—	—
Median SUV_{max} (range)	3.3 (2.2-16.8)	3.6 (2.2-9.8)	—	0.689
Mean ± SD	4.48±2.87	4.06±1.92	—	—

FAPI: Fibroblast activation protein inhibitor, SUV_{max}: Maximum standardized uptake value, SD: Standard deviation, ^{18}F-FDG PET/CT: ^{18}F-fluorodeoxyglucose positron emission tomography/computed tomography

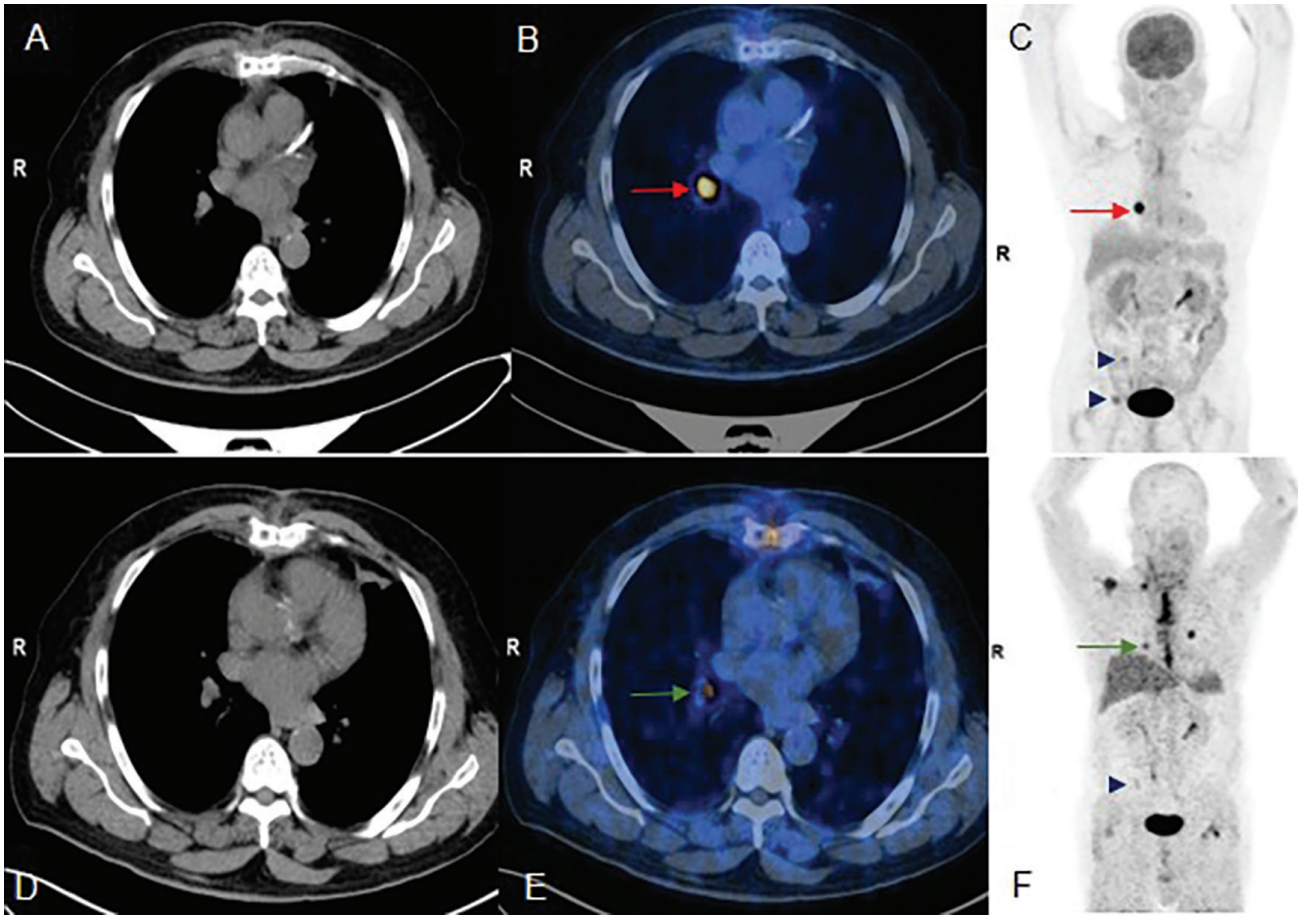

Figure 4. Representative images showing pulmonary metastases. (A, D) axial CT image showing a right lung nodule. (B) Corresponding fused ^{18}F-FDG PET image demonstrate intense metabolic activity (SUV_{max} 15.9) in the lung nodule (red arrow). (E) Fused ^{68}Ga-FAPI-04 PET image show moderate uptake (SUV_{max} 7.3) in the same nodule (green arrow). (C, F) MIP images of ^{18}F-FDG and FAPI whole body PET show additional foci of increased ^{18}F-FDG and FAPI uptake in left lung and right lower cervical lymphnode (more prominent on FAPI). Bone lesions in right iliac bone are better appreciable on ^{18}F-FDG (blue arrow heads)

^{18}F-FDG: ^{18}F-fluorodeoxyglucose, CT: Computed tomography, ^{68}Ga-FAPI PET: Gallium-68- fibroblast activation protein inhibitor positron emission tomography, SUV_{max}: Maximum standardized uptake value

Table 5. SUV_{max} values for distant metastases

	Metric	^{18}F-FDG PET/CT	^{68}Ga-FAPI PET CT
Lungs	n (detected)	5	4
	Median SUV_{max}	3.3	5.05
	mean ± SD	5.72±5.75	5.95±4.13
Bones	n (detected)	2	2
	Median SUV_{max}	4.75	3.5
	mean ± SD	4.75±0.64	3.5±0.42
Combined	Wilcoxon p-value	1.0 (not significant)	

FAPI: Fibroblast activation protein inhibitor, SUV_{max}: Maximum standardized uptake value, SD: Standard deviation, ^{18}F-FDG PET/CT: ^{18}F-fluorodeoxyglucose positron emission tomography/computed tomography, ^{68}Ga-FAPI PET: Gallium-68- fibroblast activation protein inhibitor positron emission tomography computed tomography

Discussion

This prospective comparative study of ^{18}F-FDG and ^{68}Ga-FAPI PET/CT in a representative TENIS cohort demonstrated important differences in tracer performance, especially in nodal detection. ^{18}F-FDG was positive in a significantly higher number of lymph node metastases than ^{68}Ga-FAPI (23 vs. 14 nodes, 69.7% vs. 42.4% detection rate), reaffirming its established role as the preferred modality for the evaluation of TENIS (2,3,4). These findings are consistent with large meta-analyses and practice guidelines emphasizing the sensitivity of ^{18}F-FDG PET/CT for metabolically active, dedifferentiated recurrent disease (5,6).

Clinical Significance of Nodal Detection in Papillary Thyroid Carcinoma

Papillary thyroid carcinoma characteristically metastasizes to the cervical lymph nodes, with nodal involvement occurring in 30-80% of cases, depending on tumor size and histologic features (22,23). Accurate nodal detection is critical for staging, prognostication, and treatment planning. In this context, the superior nodal detectability of ^{18}F-FDG PET/CT (23 nodes detected vs. 14 by ^{68}Ga-FAPI) represents a clinically significant advantage that directly impacts patient management decisions regarding surgical intervention, empirical radioiodine therapy, or watchful waiting (24,25).

Lesion Confirmation and Validation

The multimodal lesion confirmation approach employed in this study reflects the real-world challenges of validating imaging findings in patients with advanced TC. While 75% (9 of 12) of cervical lymph node cases were confirmed by histopathology or cytopathology, which provided robust validation, the remaining nodal lesions and most distant lesions relied on biochemical response, imaging progression, or clinical correlation. This hierarchical validation strategy, although pragmatic and clinically appropriate, limits the ability to definitively establish false-negative rates. The high proportion of histopathologically confirmed cervical nodes strengthens confidence in our finding of superior nodal detectability with ^{18}F-FDG, as these represent the most rigorously validated lesions in our cohort. For distant lesions, reliance on imaging progression and clinical correlation may introduce uncertainty but remains consistent with accepted clinical practice in managing advanced DTC, where biopsy is often impractical (26,27).

Comparative Performance of ^{18}F-FDG and ^{68}Ga-FAPI PET/CT

^{68}Ga-FAPI PET/CT, targeting fibroblast activation in the tumor microenvironment, demonstrated comparable SUV_{max} values to those of ^{18}F-FDG in paired local, nodal, and distant lesions, but failed to detect several cervical lymph nodes with metastases. This is consistent with recent reports highlighting that, while ^{68}Ga-FAPI excels in certain stroma-rich or desmoplastic lesions (especially at the local recurrence site or in some distant metastases), it is less sensitive for varied nodal disease burden (16,18,28). The mechanism underlying this differential performance is likely related to heterogeneity in the composition of the tumor microenvironment. Lymph node metastases may have lower stromal FAP expression relative to their metabolic activity, which favors ^{18}F-FDG detection (29,30).

In our analysis, distant lesions in the lungs and bones were detected by both tracers at similar detection rates. One pulmonary lesion was negative for ^{68}Ga-FAPI. The SUV_{max} values showed no significant differences (p=1.0). However, these two tracers may have different strengths. ^{68}Ga-FAPI can outperform ^{18}F-FDG in fibrotic or cancer-associated fibroblast-rich metastatic foci, as shown in recent clinical trials (21); however, it is not uniformly superior across all lesion types. The occasional higher ^{68}Ga-FAPI SUV_{max} in some locally recurrent lesions (maximum 10.5 vs. 6.8 for ^{18}F-FDG) suggests that ^{68}Ga-FAPI may identify lesions with prominent stromal reactions that could be underestimated by FDG alone (31,32).

Semiquantitative Analysis

The lack of a significant difference in uptake intensity (SUV_{max}) between ^{18}F-FDG and ^{68}Ga-FAPI in paired lesions (p=0.689 for lymph nodes, p=1.0 for distant metastases) suggests that both tracers detect lesions and provide a comparable semiquantitative assessment. This finding indicates that ^{68}Ga-FAPI can be reliably used to characterize lesions. However, the clinical impact of missing lesions—particularly the nine additional lymph nodes detected only by^{18}F-FDG (27% of all nodes) in our cohort—underscores the greater utility of ^{18}F-FDG for comprehensive restaging and treatment planning. Missed nodal disease can lead to understaging and inadequate treatment selection, potentially affecting long-term outcomes (33,34).

Comparison with Existing Literature

Our findings align with and extend those of recent comparative studies of ^{18}F-FDG and ^{68}Ga-FAPI PET/CT in TC. A recent study by Alevroudis et al. (21) reported that ^{68}Ga-FAPI detected additional lesions in approximately 20% of patients with RAIR-DTC with higher target-to-background ratios. However, that study included a broader RAIR-DTC population rather than focusing specifically on TENIS syndrome. Our study specifically addresses the TENIS population and demonstrates that, while ^{68}Ga-FAPI may

offer complementary information in select cases, ^{18}F-FDG provides superior overall lesion detection, particularly for nodal disease.

Clinical Implications and Future Directions

Based on our findings, ^{18}F-FDG PET/CT should remain the first-line imaging modality for TENIS syndrome evaluation. ^{68}Ga-FAPI PET/CT may serve as a complementary tool in specific scenarios, including when ^{18}F-FDG PET/CT is negative or equivocal despite high Tg levels; for evaluating local recurrence where stromal reaction may be prominent; in patients with poorly differentiated or dedifferentiated TC with suspected high stromal content; and for treatment planning when targeting stromal components with novel therapies.

Future research should focus on larger multicenter prospective studies to validate these findings and to establish clear clinical algorithms; to assess the correlation of ^{68}Ga-FAPI uptake with histopathologic FAP expression and stromal density; to explore ^{68}Ga-FAPI PET/CT for response assessment following targeted therapies; and to develop radiomic and artificial intelligence approaches that integrate multi-tracer PET data for improved diagnostic accuracy and prognostication.

Study Limitations

This study has a few limitations. First, the modest sample size (n=22) from a single center limits the generalizability and statistical power of the subgroup analyses. Technical factors, including different acquisition protocols for ^{18}F-FDG and ^{68}Ga-FAPI (1 vs. 2 min per bed position), may influence image quality and lesion detection, although these protocols reflect standard clinical practice for each tracer. The study was also limited by the heterogeneity of the validation methods. Finally, we did not perform a detailed analysis of the target-to-background ratios or assess the impact of lesion size on detectability, which could provide additional insights into the relative tracer performance.

Conclusion

^{18}F-FDG PET/CT remains the reference imaging modality for detecting structural disease in TENIS syndrome, while ^{68}Ga-FAPI PET/CT is a promising, currently supplementary tool when conventional imaging is inconclusive. The superior nodal detectability of ^{18}F-FDG PET/CT has direct clinical implications for the accurate staging and treatment planning of papillary thyroid carcinoma, the predominant histologic type in TENIS syndrome. The integration of both modalities, potentially in a dual-tracer protocol, could be explored to further enhance diagnostic yield and therapeutic guidance in challenging DTC cases.

Ethics

Ethics Committee Approval: The study protocol was approved by the Amrita Institute of Medical Sciences and Research Institutional Clinical Research Ethics Committee (approval number: ECASM-AIMS-2023-066, date: 24.02.2023).

Informed Consent: All patients participating in the study provided written informed consent.

Footnotes

Authorship Contributions

Concept: J.B.B., M.S., U.M., P.S., Design: J.B.B., M.S., U.M., S.S.P., Data Collection or Processing: J.B.B., P.P., A.S., S.S., B.R.R., P.S., Analysis or Interpretation: J.B.B., M.S., U.M., R.R., Literature Search: J.B.B., R.R., A.S., S.S., B.R.R., P.S., Writing: J.B.B., M.S., B.R.R., P.S.

Conflict of Interest: No conflict of interest was declared by the authors.

Financial Disclosure: The authors declared that this study has received financial support.

References

1. Siegel RL, Miller KD, Wagle NS, Jemal A. Cancer statistics, 2023. CA Cancer J Clin. 2023;73:17-48.
2. Cabanillas ME, McFadden DG, Durante C. Thyroid cancer. Lancet. 2016;388:2783-2795.
3. Haugen BR, Alexander EK, Bible KC, Doherty GM, Mandel SJ, Nikiforov YE, Pacini F, Randolph GW, Sawka AM, Schlumberger M, Schuff KG, Sherman SI, Sosa JA, Steward DL, Tuttle RM, Wartofsky L. 2015 American Thyroid Association Management Guidelines for Adult Patients with Thyroid Nodules and Differentiated Thyroid Cancer: The American Thyroid Association Guidelines Task Force on Thyroid Nodules and Differentiated Thyroid Cancer. Thyroid. 2016;26:1-133.
4. Tuttle RM, Ahuja S, Avram AM, Bernet VJ, Bourguet P, Daniels GH, Dillehay G, Draganescu C, Flux G, Führer D, Giovanella L, Greenspan B, Luster M, Muylle K, Smit JWA, Van Nostrand D, Verburg FA, Hegedüs L. Controversies, consensus, and collaboration in the use of ^{131}I therapy in differentiated thyroid cancer: a joint statement from the American Thyroid Association, the European Association of Nuclear Medicine, the Society of Nuclear Medicine and Molecular Imaging, and the European Thyroid Association. Thyroid. 2019;29:461-470.
5. Lim H, Devesa SS, Sosa JA, Check D, Kitahara CM. Trends in thyroid cancer incidence and mortality in the United States, 1974-2013. JAMA. 2017;317:1338-1348.
6. Vaisman F, Tuttle RM. Clinical assessment and follow-up of differentiated thyroid cancer patients. Best Pract Res Clin Endocrinol Metab. 2013;27:503-512.
7. Durante C, Haddy N, Baudin E, Leboulleux S, Hartl D, Travagli JP, Caillou B, Ricard M, Lumbroso JD, De Vathaire F, Schlumberger M. Long-term outcome of 444 patients with distant metastases from papillary and follicular thyroid carcinoma: benefits and limits of radioiodine therapy. J Clin Endocrinol Metab. 2006;91:2892-2899.
8. Schlumberger M, Tahara M, Wirth LJ, Robinson B, Brose MS, Elisei R, Habra MA, Newbold K, Shah MH, Hoff AO, Gianoukakis AG, Kiyota N, Taylor MH, Kim SB, Krzyzanowska MK, Dutcus CE, de las Heras B, Zhu

J, Sherman SI. Lenvatinib versus placebo in radioiodine-refractory thyroid cancer. N Engl J Med. 2015;372:621-630.

9. Xing M, Haugen BR, Schlumberger M. Progress in molecular-based management of differentiated thyroid cancer. Lancet. 2013;381:1058-1069.
10. Robbins RJ, Larson SM, Sinha N, Shaha A, Divgi C, Pentlow KS, et al. A retrospective review of the role of FDG-PET in the management of patients with metastatic thyroid cancer. J Clin Endocrinol Metab. 2006;91:498-505.
11. Feine U, Lietzenmayer R, Hanke JP, Held J, Wöhrle H, Müller-Schauenburg W. Fluorine-18-FDG and iodine-131-iodide uptake in thyroid cancer. J Nucl Med. 1996;37:1468-1472.
12. Wang W, Larson SM, Fazzari M, Tickoo SK, Kolbert K, Sgouros G, Yeung H, Macapinlac H, Rosai J, Robbins RJ. Prognostic value of [^{18}F] fluorodeoxyglucose positron emission tomographic scanning in patients with thyroid cancer. J Clin Endocrinol Metab. 2000;85:1107-1113.
13. Robbins RJ, Schlumberger MJ. The evolving role of (131)I for the treatment of differentiated thyroid carcinoma. J Nucl Med. 2005;46 Suppl 1:28S-37S.
14. Palmedo H, Bucerius J, Joe A, Strunk H, Hortling N, Meyka S, Roedel R, Wolff M, Wardelmann E, Biersack HJ, Jaeger U. Integrated PET/CT in differentiated thyroid cancer: diagnostic accuracy and impact on patient management. J Nucl Med. 2006;47:616-624.
15. Miller ME, Wang P, Tuttle RM, Grewal RK. FDG-PET in papillary thyroid carcinoma: a systematic review and meta-analysis. Head Neck. 2011;33:562-565.
16. Kratochwil C, Flechsig P, Lindner T, Abderrahim L, Altmann A, Mier W, Adeberg S, Rathke H, Röhrich M, Winter H, Plinkert PK, Marme F, Lang M, Kauczor HU, Jäger D, Debus J, Haberkorn U, Giesel FL. ^{68}Ga-FAPI PET/CT: tracer uptake in 28 different kinds of cancer. J Nucl Med. 2019;60:801-805.
17. Giesel FL, Kratochwil C, Lindner T, Marschalek MM, Loktev A, Lehnert W, Debus J, Jäger D, Flechsig P, Altmann A, Mier W, Haberkorn U. ^{68}Ga-FAPI PET/CT: biodistribution and preliminary dosimetry estimate of 2 DOTAContaining FAP-targeting agents in patients with various cancers. J Nucl Med. 2019;60:386-392.
18. Shi X, Xing H, Yang X, Li F, Yao S, Zhang H, Zhao H, Hacker M, Huo L, Li X. Fibroblast imaging of hepatic carcinoma with ^{68}Ga-FAPI-04 PET/CT: a pilot study in patients with suspected hepatic nodules. Eur J Nucl Med Mol Imaging. 2021;48:196-203.
19. Pang Y, Zhao L, Luo Z, Hao B, Wu H, Lin Q, Sun L, Chen H. Comparison of ^{68}Ga-FAPI and ^{18}F-FDG uptake in gastric, duodenal, and colorectal cancers. Radiology. 2021;298:393-402.
20. Ballal S, Yadav MP, Moon ES, Kramer VS, Roesch F, Kumari S, Tripathi M, ArunRaj ST, Sarswat S, Bal C. Biodistribution, pharmacokinetics, dosimetry of [^{68}Ga]Ga-DOTA.SA.FAPi, and the head-to-head comparison with [^{18}F]F-FDG PET/CT in patients with various cancers. Eur J Nucl Med Mol Imaging. 2021;48:1915-1931.
21. Alevroudis E, Skoura E, Skarlatos A, Gkika E, Exadaktylos N, Zissimopoulos A, et al. Head-to-head comparison of [^{18}F]FDG and [^{68}Ga]Ga-FAPI-74 PET/CT in radioiodine-refractory differentiated thyroid cancer. Eur J Nucl Med Mol Imaging. 2024;51(Suppl 1):S102.
22. Leboulleux S, Girard E, Rose M, Travagli JP, Sabbah N, Caillou B, Hartl DM, Lassau N, Baudin E, Schlumberger M. Ultrasound criteria of malignancy for cervical lymph nodes in patients followed up for differentiated thyroid cancer. J Clin Endocrinol Metab. 2007;92:3590-3594.
23. Adam MA, Pura J, Gu L, Dinan MA, Tyler DS, Reed SD, et al. Extent of surgery for papillary thyroid cancer is not associated with survival: an analysis of 61,775 patients. J Clin Oncol. 2015;33:2370-2375.
24. Rondeau G, Fish S, Hann LE, Fagin JA, Tuttle RM. Ultrasonographically detected small thyroid bed nodules identified after total thyroidectomy for differentiated thyroid cancer seldom show clinically significant structural progression. Thyroid. 2011;21:845-853.
25. Robenshtok E, Grewal RK, Fish S, Sabra MM, Tuttle RM. Thyroglobulin antibody status and ^{131}I whole-body scan results predict the need for further radioiodine therapy in patients with low stimulated thyroglobulin levels. Thyroid. 2013;23;23:436-442.
26. Schlumberger M, Tubiana M, De Vathaire F, Hill C, Gardet P, Travagli JP, et al. Long-term results of treatment of 283 patients with lung and bone metastases from differentiated thyroid carcinoma. J Nucl Med. 1996;37:598-605.
27. Farooki A, Leung V, Tala H, Tuttle RM. Skeletal-related events due to bone metastases from differentiated thyroid cancer. J Clin Endocrinol Metab. 2012;97:2433-2439.
28. Wang Y, Chen L, Liu X, Zhao L, Sun X, Luo Z, et al. Fibroblast activation protein expression in thyroid cancer and its clinical significance. Front Med (Lausanne). 2023;10:1279978.
29. Sahai E, Astsaturov I, Cukierman E, DeNardo DG, Egeblad M, Evans RM, Fearon D, Greten FR, Hingorani SR, Hunter T, Hynes RO, Jain RK, Janowitz T, Jorgensen C, Kimmelman AC, Kolonin MG, Maki RG, Powers RS, Puré E, Ramirez DC, Scherz-Shouval R, Sherman MH, Stewart S, Tlsty TD, Tuveson DA, Watt FM, Weaver V, Weeraratna AT, Werb Z. A framework for advancing our understanding of cancer-associated fibroblasts. Nat Rev Cancer. 2020;20:174-186.
30. Kalluri R. The biology and function of fibroblasts in cancer. Nat Rev Cancer. 2016;16:582-598.
31. Lindner T, Loktev A, Altmann A, Giesel F, Kratochwil C, Debus J, Jäger D, Mier W, Haberkorn U. Development of quinoline-based theranostic ligands for the targeting of fibroblast activation protein. J Nucl Med. 2018;59:1415-1422.
32. Mona CE, Benz MR, Hikmat F, Grogan TR, Lueckerath K, Razmaria A, Riahi R, Slavik R, Girgis MD, Carlucci G, Kelly KA, French SW, Czernin J, Dawson DW, Calais J. Correlation of ^{68}Ga-FAPi-46 PET biodistribution with FAP expression by immunohistochemistry in patients with solid cancers: interim analysis of a prospective translational exploratory study. J Nucl Med. 2022;63:1021-1026.
33. Hay ID, Thompson GB, Grant CS, Bergstralh EJ, Dvorak CE, Gorman CA, Maurer MS, McIver B, Mullan BP, Oberg AL, Powell CC, van Heerden JA, Goellner JR. Papillary thyroid carcinoma managed at the Mayo Clinic during six decades (1940-1999): temporal trends in initial therapy and long-term outcome in 2444 consecutively treated patients. World J Surg. 2002;26:879-885.
34. Nixon IJ, Wang LY, Palmer FL, Tuttle RM, Shaha AR, Shah JP, et al. The impact of age on risk stratification for thyroid cancer. Thyroid. 2016;26:373-380.